

A comparison framework for temporal image reconstructions in electrical impedance tomography

Hervé Gagnon¹, Bartłomiej Grychtol² and Andy Adler¹

¹ Department of Systems and Computer Engineering, Carleton University, Ottawa, K1S 5B6, Canada

² Fraunhofer Project Group for Automation in Medicine and Biotechnology, Mannheim, Germany

E-mail: adler@sce.carleton.ca

Abstract. Electrical impedance tomography (EIT) provides low-resolution images of internal conductivity distributions, but is able to achieve relatively high temporal resolutions. Most EIT image reconstruction algorithms do not explicitly account for the temporal constraints on the measurements or physiological processes under investigation. Instead, algorithms typically assume both that the conductivity distribution does not change during the acquisition of each EIT data frame, and that frames can be reconstructed independently, without consideration of the correlation between images. A failure to account for these temporal effects will result in aliasing-related artefacts in images. Several methods have been proposed to compensate for these effects, including interpolation of raw data, and reconstruction algorithms using Kalman and temporal filtering. However, no systematic work has been performed to understand the severity of the temporal artefacts nor the extent to which algorithms can account for them. We seek to address this need by developing a temporal comparison framework and figures of merit (FOM) to assess the ability of reconstruction algorithms to account for temporal effects. Using this approach, we compare combinations of three reconstruction algorithms using three EIT data frame types: perfect, realistic, and interpolated. Results show that, without accounting for temporal effects, artefacts are present in images for dynamic conductivity contrasts at frequencies 10 to 20 times slower than the frame rate. The proposed methods show some improvements in reducing these artefacts.

Keywords: electrical impedance tomography, image reconstruction algorithm, comparison framework, figures of merit

1. Introduction

Electrical impedance tomography (EIT) calculates images of internal conductivity distributions from body surface measurements. Currently, the most promising application of EIT is real-time monitoring of pulmonary ventilation (Adler *et al* 2012). Compared to other medical imaging techniques, EIT has relatively low spatial resolution but high temporal resolution. Commercially available lung monitoring EIT systems (Draeger AG 2010, Swisstom AG 2014) are able to reconstruct and display images in

real time at up to 50 frames/second. Faster EIT systems have been developed for other applications such as the fEITER system for functional brain imaging working at up to 100 frames/second (McCann *et al* 2011).

EIT requires performing transimpedance measurements, typically from a set of 16 or 32 electrodes placed around the region of interest, such as the torso for monitoring lung ventilation. From a set of electrodes, measurements are performed by applying a current through a pair of electrodes while performing voltage measurements using all other remaining electrodes pairs, and then switching the current stimulation to another pair of electrodes in a sequential process. A complete set of independent measurements is called a frame, from which an EIT image is calculated via a reconstruction algorithm.

Most EIT image reconstruction algorithms make the assumption that the conductivity distribution does not change during the acquisition of an entire EIT frame. This is of course an approximation since the lungs are breathing and the heart is beating during the sequential process of data acquisition. This assumption is valid only if the frame rate is much higher than the rate of physiological conductivity changes inside the body area of interest. Yerworth and Bayford (2013) have suggested a ratio of 50 between frame rate and the highest frequency component should be sufficient. For EIT of the torso, the fastest expected physiological impedance changes would come from heart activity (fundamental frequency up to 220 beats/minute or 3.67 beats/second) and high frequency oscillatory ventilation (HFOV) (fundamental frequency up to 60 Hz). Harmonics of those fundamental frequencies may also cause aliasing artefacts.

Furthermore, in most reconstruction algorithms proposed, EIT frames are independently reconstructed in a series of EIT images, as if there were no correlation between successive EIT images. A few authors, however, have proposed innovative methods to account for the fact that the conductivity distribution varies during the acquisition of an EIT frame and/or the fact that successive EIT images are correlated with one another, especially at high frame rates. Vauhkonen *et al* (1998) first proposed using a Kalman filter approach to reconstruct EIT images to account for the temporal correlation between successive EIT images. Other groups, such as Trigo *et al* (2004) and Kim *et al* (2006), have further worked on refining and adapting the Kalman filter approach to different scenarios. Adler *et al* (2007) first proposed a temporal reconstruction algorithm that accounts for temporal correlation by reconstructing EIT images while considering a total of $2d + 1$ data frames, corresponding to the current frame, d anterior frames and d posterior frames. More recently, Yerworth and Bayford (2013) first proposed interpolating EIT measurements to account for the fact that measurements in a frame are not acquired simultaneously. Related methods have also been proposed by other groups, such as Voutilainen *et al* (2012), in the process tomography field.

Although all these propositions seem promising, no comparison framework has been proposed to assess the benefits and compare each of the proposed methods. In this paper, we develop a comparison framework to measure the ability of EIT reconstruction algorithms to account for temporal effects – the fact that measurements within a frame

are not synchronous. Three reconstruction algorithms are presented: 1) Gauss-Newton formulation, 2) temporal reconstruction algorithm, and 3) Kalman filter formulation. Three types of EIT data frames are then defined: 1) perfect, 2) realistic, and 3) interpolated. Finally, the comparison criteria are defined as an extension of the figures of merit (FOM) proposed as part of the GREIT algorithm. Comparison results are then presented and analysed.

2. Methods

EIT systems used for monitoring lung ventilation acquire transimpedance data from a set of n_e (typically 16 or 32) electrodes, typically uniformly spaced around the torso. The most common data acquisition pattern is the Sheffield protocol, which consists of applying current through an adjacent pair of electrodes while measuring voltages using all remaining adjacent pairs of electrodes, and then repeating current application through the next adjacent electrode pair. It provides $n_m = n_e(n_e - 3)$ measurements, half of which are independent, which constitutes an EIT data frame $\mathbf{v} \in \mathbb{R}^{n_m}$. For a typical 16-electrode EIT system, $n_m = 208$.

Most EIT systems reconstruct time difference images (TDI) that represent the variation in conductivity distribution between the current frame, \mathbf{v} , and a reference frame, \mathbf{v}_r . \mathbf{v}_r typically corresponds to an average measurement, or a time such as end-expiration where the conductivity is relatively stable. TDI requires difference data $\mathbf{y} \in \mathbb{R}^{n_m}$ defined as $\mathbf{y} = \mathbf{v} - \mathbf{v}_r$, or normalized difference data, $\mathbf{y} = (\mathbf{v} - \mathbf{v}_r)/\mathbf{v}_r$ (where the division operator $/$ is meant as vector-element by vector-element division). For TDI, $\mathbf{x} \in \mathbb{R}^{n_n}$ represents variations in conductivity distribution between two instants, $\boldsymbol{\sigma} - \boldsymbol{\sigma}_r$, where n_n is the number of pixels or finite element model (FEM) elements in the image.

For small conductivity variations around $\boldsymbol{\sigma}_r$, the relationship between the difference data \mathbf{y} and image \mathbf{x} is obtained from the forward problem:

$$\mathbf{y} = \mathbf{J}\mathbf{x} + \mathbf{n} \quad (1)$$

where $\mathbf{J} \in \mathbb{R}^{n_m \times n_n}$ is the sensitivity matrix or Jacobian and $\mathbf{n} \in \mathbb{R}^{n_m}$ is random measurement noise assumed to be zero-mean Gaussian distributed. \mathbf{J} is typically calculated using the FEM and depends on the geometry, stimulating current patterns, reference conductivity distribution, and electrode model. The inverse problem of calculating \mathbf{x} knowing \mathbf{y} , the geometry, stimulating patterns, and electrode model, is ill-conditioned.

2.1. Image Reconstruction Algorithms

2.1.1. Gauss-Newton Formulation Most non-temporal EIT reconstruction algorithms can be represented in terms of Tikhonov regularization, where the solution $\hat{\mathbf{x}}$ minimizes:

$$\hat{\mathbf{x}} = \arg \min_{\mathbf{x}} \left[\|\mathbf{y} - \mathbf{J}\mathbf{x}\|_{\mathbf{\Gamma}_n^{-1}}^2 + \lambda^2 \|\mathbf{x} - \mathbf{x}_0\|_{\mathbf{\Gamma}_x^{-1}}^2 \right] \quad (2)$$

where \mathbf{x}_0 is the expected conductivity change (usually zero for TDI). $\mathbf{\Gamma}_n \in \mathbb{R}^{n_m \times n_m}$ is the measurement noise covariance matrix and $\mathbf{\Gamma}_x \in \mathbb{R}^{n_n \times n_n}$ is the expected image covariance matrix. $\lambda \in \mathbb{R}$ is an hyperparameter adjusting the weighting between both norms.

Solving (2), we obtain:

$$\hat{\mathbf{x}} = \left((\mathbf{J}^T \mathbf{\Gamma}_n^{-1} \mathbf{J} + \lambda^2 \mathbf{\Gamma}_x^{-1})^{-1} \mathbf{J}^T \mathbf{\Gamma}_n^{-1} \right) \mathbf{y} = \mathbf{B} \mathbf{y} \quad \text{Classical form} \quad (3)$$

$$\hat{\mathbf{x}} = \left(\mathbf{\Gamma}_x \mathbf{J}^T (\mathbf{J} \mathbf{\Gamma}_x \mathbf{J}^T + \lambda^2 \mathbf{\Gamma}_n)^{-1} \right) \mathbf{y} = \mathbf{B} \mathbf{y} \quad \text{Wiener filter form} \quad (4)$$

where \mathbf{B} is the reconstruction matrix. Since measurement noise is usually uncorrelated, covariance matrix $\mathbf{\Gamma}_n$ is typically set to a diagonal matrix. Covariance matrix $\mathbf{\Gamma}_x$, is usually assembled in its inverse form $\mathbf{\Gamma}_x^{-1} = \mathbf{F}^T \mathbf{F}$ to emphasize in matrix \mathbf{F} what is not desirable in the final conductivity distribution (Adler and Guardo 1996).

2.1.2. Temporal Reconstruction Algorithm A temporal reconstruction algorithm (Adler *et al* 2007) was proposed to account for the temporal correlation in successive EIT data frames and images. An extended difference data vector $\tilde{\mathbf{y}}_t$ is defined at time t as the vertical concatenation of the d previous, current and d future data frames. The corresponding extended conductivity variation $\tilde{\mathbf{x}}_t$ is similarly defined. Equation (1) expressed with these extended vectors then becomes

$$\underbrace{\begin{bmatrix} \mathbf{y}_{t-d} \\ \vdots \\ \mathbf{y}_t \\ \vdots \\ \mathbf{y}_{t+d} \end{bmatrix}}_{\tilde{\mathbf{y}}_t} = \underbrace{\begin{bmatrix} \mathbf{J} & \cdots & \mathbf{0} \\ & \ddots & \\ \vdots & \mathbf{J} & \vdots \\ & & \ddots \\ \mathbf{0} & \cdots & \mathbf{J} \end{bmatrix}}_{\tilde{\mathbf{J}}} \underbrace{\begin{bmatrix} \mathbf{x}_{t-d} \\ \vdots \\ \mathbf{x}_t \\ \vdots \\ \mathbf{x}_{t+d} \end{bmatrix}}_{\tilde{\mathbf{x}}_t} + \underbrace{\begin{bmatrix} \mathbf{n}_{t-d} \\ \vdots \\ \mathbf{n}_t \\ \vdots \\ \mathbf{n}_{t+d} \end{bmatrix}}_{\tilde{\mathbf{n}}_t} \quad (5)$$

or $\tilde{\mathbf{y}}_t = \tilde{\mathbf{J}} \tilde{\mathbf{x}}_t + \tilde{\mathbf{n}}_t$ in compact form. Equations (2) and (4) then become

$$\hat{\tilde{\mathbf{x}}} = \arg \min_{\tilde{\mathbf{x}}} \left[\|\tilde{\mathbf{y}} - \tilde{\mathbf{J}} \tilde{\mathbf{x}}\|_{\mathbf{\Gamma}_{\tilde{\mathbf{n}}}}^{-1}}^2 + \lambda^2 \|\tilde{\mathbf{x}} - \tilde{\mathbf{x}}_0\|_{\mathbf{\Gamma}_{\tilde{\mathbf{x}}}}^{-1}}^2 \right] \quad (6)$$

$$\hat{\tilde{\mathbf{x}}} = \left(\mathbf{\Gamma}_{\tilde{\mathbf{x}}} \tilde{\mathbf{J}}^T (\tilde{\mathbf{J}} \mathbf{\Gamma}_{\tilde{\mathbf{x}}} \tilde{\mathbf{J}}^T + \lambda^2 \mathbf{\Gamma}_{\tilde{\mathbf{n}}})^{-1} \right) \tilde{\mathbf{y}} = \tilde{\mathbf{B}} \tilde{\mathbf{y}} \quad (7)$$

where $\tilde{\mathbf{J}} = \mathbf{I} \otimes \mathbf{J}$, \mathbf{I} is the identity matrix, and \otimes represents the Kronecker product. Since the measurement noise characteristics should be similar for all data frames, $\mathbf{\Gamma}_{\tilde{\mathbf{n}}} = \mathbf{I} \otimes \mathbf{\Gamma}_n$. The time correlation between successive frames is represented by a correlation γ with a value between 0 and 1. The matrix $\mathbf{\Gamma}$ is defined as

$$\mathbf{\Gamma} = \begin{bmatrix} 1 & \gamma & \cdots & \gamma^{2d-1} & \gamma^{2d} \\ \gamma & 1 & \cdots & \gamma^{2d-2} & \gamma^{2d-1} \\ \vdots & \vdots & \ddots & \vdots & \vdots \\ \gamma^{2d-1} & \gamma^{2d-2} & \cdots & 1 & \gamma \\ \gamma^{2d} & \gamma^{2d-1} & \cdots & \gamma & 1 \end{bmatrix}. \quad (8)$$

From this definition of $\mathbf{\Gamma}$, $\mathbf{\Gamma}_{\tilde{\mathbf{x}}} = \mathbf{\Gamma} \otimes \mathbf{\Gamma}_{\mathbf{x}}$ where $\mathbf{\Gamma}$ reflects the time correlation between successive images while $\mathbf{\Gamma}_{\mathbf{x}}$ represents spatial correlation between adjacent elements of an EIT image.

2.1.3. Kalman Filter Formulation The Kalman filter formulation expresses the forward problem as a state estimation problem, where the state vector at the k^{th} instant of a time sequence is the image \mathbf{x}_k . The state transition equation is

$$\mathbf{x}_k = \mathbf{A}\mathbf{x}_{k-1} + \mathbf{w} \quad (9)$$

where $\mathbf{A} \in \mathbb{R}^{n_n \times n_n}$ is the state transition matrix that relates the current state at time k to the previous state at time $k - 1$. Most often \mathbf{A} is set to the identity matrix which corresponds to the random walk model. Vector $\mathbf{w} \in \mathbb{R}^{n_n}$ is the state noise which is typically a zero-mean Gaussian with a covariance matrix of $\mathbf{\Gamma}_{\mathbf{w}}$ representing the modeling error of the state transition matrix.

The observation equation is obtained from (1) as

$$\mathbf{y}_k = \mathbf{J}_k \mathbf{x}_k + \mathbf{n} \quad (10)$$

A prior estimate \mathbf{x}_k^- and its covariance matrix \mathbf{P}_k^- are first calculated from (9) as

$$\mathbf{x}_k^- = \mathbf{A}\hat{\mathbf{x}}_{k-1} \quad (11)$$

$$\mathbf{P}_k^- = \mathbf{A}\hat{\mathbf{P}}_{k-1}\mathbf{A}^T + \mathbf{\Gamma}_{\mathbf{w}}. \quad (12)$$

The *a posteriori* estimate $\hat{\mathbf{x}}_k$ and its covariance matrix $\hat{\mathbf{P}}_k$ can be calculated as

$$\hat{\mathbf{x}}_k = \mathbf{x}_k^- + \mathbf{K}_k(\mathbf{y}_k - \mathbf{J}_k \mathbf{x}_k^-) \quad (13)$$

$$\hat{\mathbf{P}}_k = (\mathbf{I} - \mathbf{K}_k \mathbf{J}_k) \mathbf{P}_k^-. \quad (14)$$

where $\mathbf{K}_k = \mathbf{P}_k^- \mathbf{J}_k^T (\mathbf{J}_k \mathbf{P}_k^- \mathbf{J}_k^T + \mathbf{\Gamma}_{\mathbf{n}})^{-1}$ is the Kalman gain. Equations (11) through (14) have to be run iteratively on successive EIT data frames to reconstruct EIT images using the Kalman filter formulation.

2.2. EIT Data frames

During EIT data acquisition, the conductivity distribution varies due to physiological activities such as respiration, blood circulation and digestion. As previously stated, most EIT reconstruction algorithms assume that the conductivity does not vary during the acquisition of a data frame, $\mathbf{v} \in \mathbb{R}^{n_m}$. In fact, each measurement, $\mathbf{v}_i \in \mathbb{R}$, depends on the conductivity distribution $\boldsymbol{\sigma}$ when it is made, $v_i = f_i(\boldsymbol{\sigma}(t))$. Here, v_i is the i^{th} measurement within frame \mathbf{v} . In order to evaluate the assumptions, we define three types of EIT data frames: perfect, realistic and interpolated.

2.2.1. Perfect EIT Data Frames We define perfect EIT data frames as frames in which all EIT measurements are acquired simultaneously. EIT data frames are uniformly sampled at the frame rate ($f_f = 1/T_f$) where T_f is the time frame period. Perfect EIT data frames are therefore defined as

$$\mathbf{v}_p(nT_f) = \begin{bmatrix} v_1 \\ v_2 \\ \vdots \\ v_{n_m-1} \\ v_{n_m} \end{bmatrix} = \begin{bmatrix} f_1(\boldsymbol{\sigma}(nT_f)) \\ f_2(\boldsymbol{\sigma}(nT_f)) \\ \vdots \\ f_{n_m-1}(\boldsymbol{\sigma}(nT_f)) \\ f_{n_m}(\boldsymbol{\sigma}(nT_f)) \end{bmatrix} \quad (15)$$

where $n \in \mathbb{N}$ is an integer. Perfect EIT data frames therefore represent the type of frames most EIT reconstruction algorithms expect, where there is no change in conductivity distribution during the frame acquisition.

2.2.2. Realistic EIT Data Frames However, real EIT system cannot acquire every measurement of a frame simultaneously. Serial devices sequentially acquire all measurements, and parallel systems make simultaneous voltage measurements but sequential current stimulations. We consider a serial device where each measurement is acquired at a frequency $f_m = 1/T_m$ equal to $n_m f_f$ where n_m is the number of measurements per frame and T_m is the time necessary (including set-up and acquisition) to acquire one measurement. For some systems, T_m might vary depending on whether the current injecting electrodes are commuted or not for one particular measurement. Here, we assume T_m to be constant.

We define a realistic EIT data frames to be sampled at the frame rate ($f_f = 1/T_f$) where T_f corresponds to the time period between adjacent frames.

$$\mathbf{v}_r(nT_f) = \begin{bmatrix} v_1 \\ v_2 \\ \vdots \\ v_{n_m-1} \\ v_{n_m} \end{bmatrix} = \begin{bmatrix} f_1(\boldsymbol{\sigma}(nT_f)) \\ f_2(\boldsymbol{\sigma}(nT_f + T_m)) \\ \vdots \\ f_{n_m-1}(\boldsymbol{\sigma}(nT_f + (n_m - 2)T_m)) \\ f_{n_m}(\boldsymbol{\sigma}(nT_f + (n_m - 1)T_m)) \end{bmatrix} \quad (16)$$

where $n \in \mathbb{N}$ is an integer. Realistic EIT data frames represent those obtained from a serial EIT system. We later show the artefacts from reconstruction algorithms that do not account for temporal effects.

2.2.3. Interpolated EIT Data Frames Yerworth and Bayford (2013) proposed interpolation of EIT measurements in order to reduce artefacts in EIT images from time-varying conductivities. Linear and frequency-domain interpolation strategies were defined. Using linear interpolation, an interpolated EIT data frame $\mathbf{v}_i(nT_f)$ is calculated from successive realistic EIT data frames $\mathbf{v}_r((n-1)T_f)$ and $\mathbf{v}_r(nT_f)$ as

$$[\mathbf{v}_i(nT_f)]_i = \frac{(i-1)[\mathbf{v}_r((n-1)T_f)]_i + (n_m - (i-1))[\mathbf{v}_r(nT_f)]_i}{n_m} \quad (17)$$

2.3. Performance Figures of Merit

While no figures of merit (FOM) have been defined to assess the performance of temporal EIT image reconstruction algorithms, several FOM have been defined for non-temporal reconstruction algorithms as part of the GREIT algorithm (Adler *et al* 2009). We summarize their definition, and extend them for temporal EIT reconstruction algorithms in the following section.

2.3.1. GREIT Figures of Merit: Five FOM were defined, in order of perceived importance. Each FOM is calculated from a reconstructed image of a small (5% of the medium diameter) spherical conductive target located at a distance r_t from the medium centre. From the reconstructed image $\hat{\mathbf{x}}$, a one-fourth amplitude binary image $\hat{\mathbf{x}}_q$ is defined as all pixels exceeding $\frac{1}{4}$ of the image maximum.

- Amplitude response (AR) is the ratio of pixel amplitudes in the reconstructed image to the conductivity contrast of the target.

$$\text{AR} = \frac{\sum_k [\hat{\mathbf{x}}]_k}{V_t \frac{\Delta\sigma}{\sigma_r}} \quad (18)$$

where k represents the k^{th} pixel, V_t is the target size (volume or area), σ_t and σ_r are the conductivities of the target and medium background, and $\Delta\sigma = \sigma_t - \sigma_r$.

- Position error (PE) is the difference between the expected target position r_t and its position in the reconstructed image $\hat{\mathbf{x}}$.

$$\text{PE} = r_t - r_q \quad (19)$$

where r_q is defined as the centre of gravity of binary image $\hat{\mathbf{x}}_q$.

- Resolution (RES) evaluates the size of the reconstructed target as a fraction of the medium size.

$$\text{RES} = \sqrt{\frac{A_q}{A_0}} \quad (20)$$

where $A_q = \sum_k [\hat{\mathbf{x}}_q]_k$ is the number of one-pixels in $\hat{\mathbf{x}}_q$ and A_0 is the number of valid pixels, which corresponds to the area in pixels of the entire reconstructed medium.

- Shape deformation (SD) represents the distortion of the small spherical conductive target from a circle in the reconstructed image.

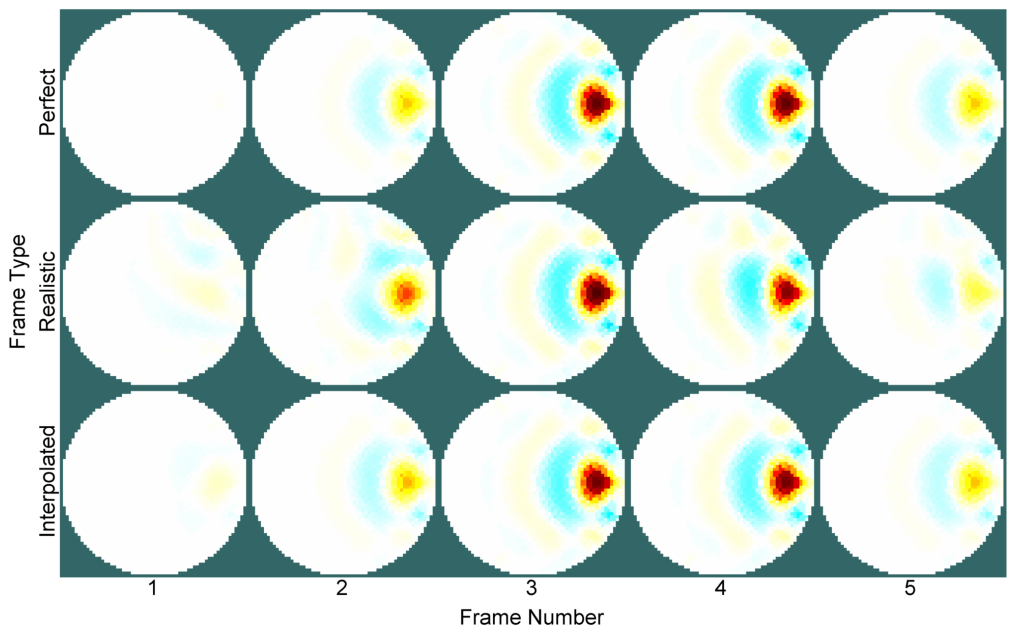
$$\text{SD} = \frac{\sum_{k \notin C} [\hat{\mathbf{x}}_q]_k}{\sum_k [\hat{\mathbf{x}}_q]_k} \quad (21)$$

where C corresponds to a circle centred at r_q with an area equivalent to A_q .

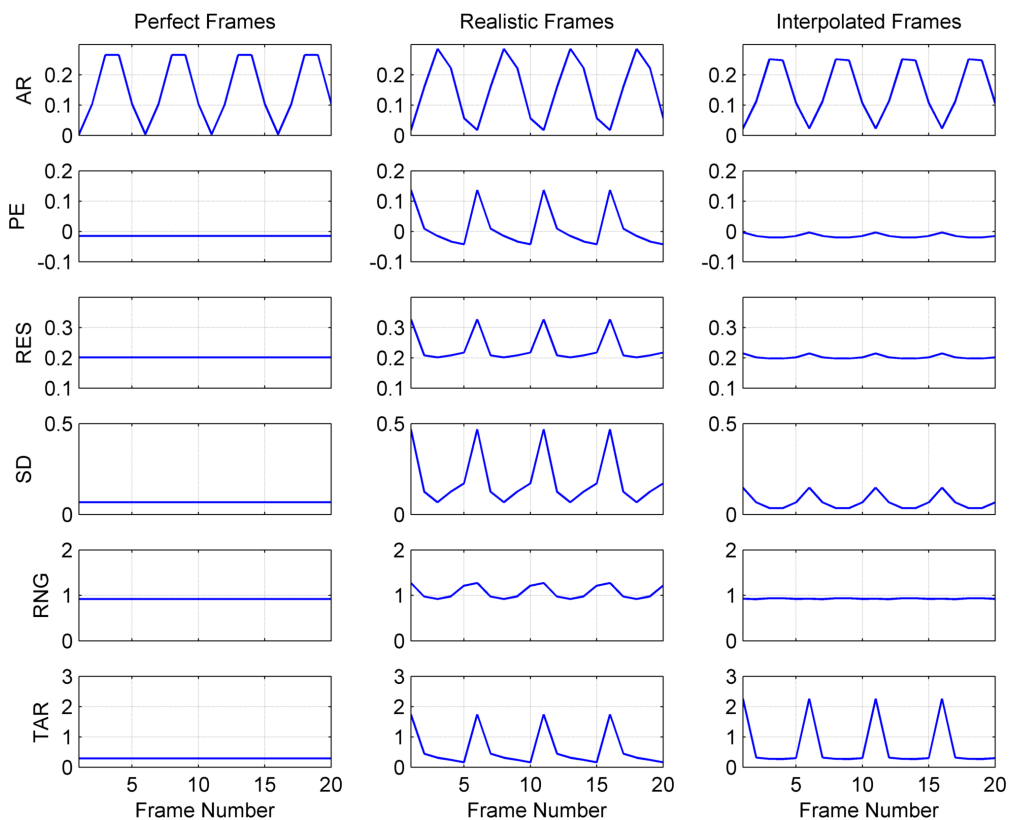
- Ringing (RNG) evaluates the extent of areas of opposite signs surrounding the main reconstructed target area.

$$\text{RNG} = \frac{\sum_{k \notin C \wedge [\hat{\mathbf{x}}_q]_k < 0} [\hat{\mathbf{x}}_q]_k}{\sum_{k \in C} [\hat{\mathbf{x}}_q]_k} \quad (22)$$

where C corresponds to a circle centred at r_q with an area equivalent to A_q .



(a)



(b)

Figure 1. (a) Sequence of images for one cycle of a sinusoidal conductivity change reconstructed with the Gauss-Newton algorithm from three different EIT data frame types: perfect (top row), realistic (middle row) and interpolated (bottom row). (b) Figures of merit calculated for four cycles of the image sequences represented in (a): 1) amplitude response (AR), 2) position error (PE), 3) resolution (RES), 4) shape deformation (SD), 5) ringing (RNG), and 6) temporal amplitude response (TAR).

2.3.2. Extension for Temporal EIT Reconstructions Figure 1(a) shows sequences of EIT images reconstructed for a target whose conductivity is sinusoidally varying at 0.2 cycles per frame for a total of one cycle, using perfect (top), realistic (middle) and interpolated (bottom) data frames. Ringing and shape deformation artefacts can clearly be seen especially in the middle sequence using realistic frames and for smaller target amplitudes. The top five rows of figure 1(b) show FOM calculated for four cycles of the three image sequences from figure 1(a) using GREIT FOM definitions. All FOM vary over time (expressed as frame number) especially for realistic frames. Except for AR, FOM do not vary for perfect frames. The GREIT definition of AR from (18) can be modified to account for that:

$$\text{TAR} = \frac{\sum_k [\hat{\mathbf{x}}]_k}{V_t \frac{\Delta\sigma(t)}{\sigma_r}} \quad (23)$$

where TAR stands for temporal amplitude response and $\Delta\sigma(t)$ is now a function of time and is adjusted according to the known sinusoidal amplitude of the conductivity target. TAR is represented on the bottom row of figure 1(b). In this case, only images reconstructed from perfect frames exhibit a constant TAR for all images of the sequence.

From observations of FOM in figure 1(b), we define for temporal image reconstruction algorithms the following extended FOM based on the FOM defined for GREIT. They will be defined as 1) TAR, 2) PE, 3) RES, 4) SD, and RNG calculated on a sequence of images reconstructed for a number of complete cycles of a sinusoidally oscillating conductivity target. The FOM will be expressed as the mean and standard-deviation over the whole sequence of images for all five FOM.

2.4. Simulations

All simulations were performed in EIDORS version 3.7.1. A 3-D FEM model of a cylinder was designed for the forward problem with the following parameters: height 2, radius 1, 55 181 elements and one 16-electrode (circular, radius 0.05) plane located at mid-height. A small spherical (radius 0.05) conductivity target located at mid-height at a radial distance r varying from 0 (medium centre) to 1 (medium boundary) was introduced in the cylinder. The background (reference) conductivity of the medium was set to 1 while the conductivity of the target σ_t was varied as a function of time as:

$$\sigma_t = 1 - \frac{\cos(2\pi f_{c/m} t_m + \phi)}{2} + 0.01 \quad (24)$$

where $f_{c/m}$ is the frequency expressed in cycles per measurement, t_m is the measurement number starting at zero for the first measurement of the first frame and ϕ represents a phase shift. The frequency expressed in cycles per frame $f_{c/f}$ is equal to $n_m f_{c/m}$ where n_m represents the number of measurements per frame. A small offset of 0.01 was added to prevent the target from reaching the same conductivity as the background and disappearing from the expected reconstructed images, which would cause numerical issues for the division in TAR. Frames are simulated for an integer number of cycles n_c to obtain a total of $n_f = n_c / f_{c/f}$ frames. FOM are computed for each of the n_f frames.

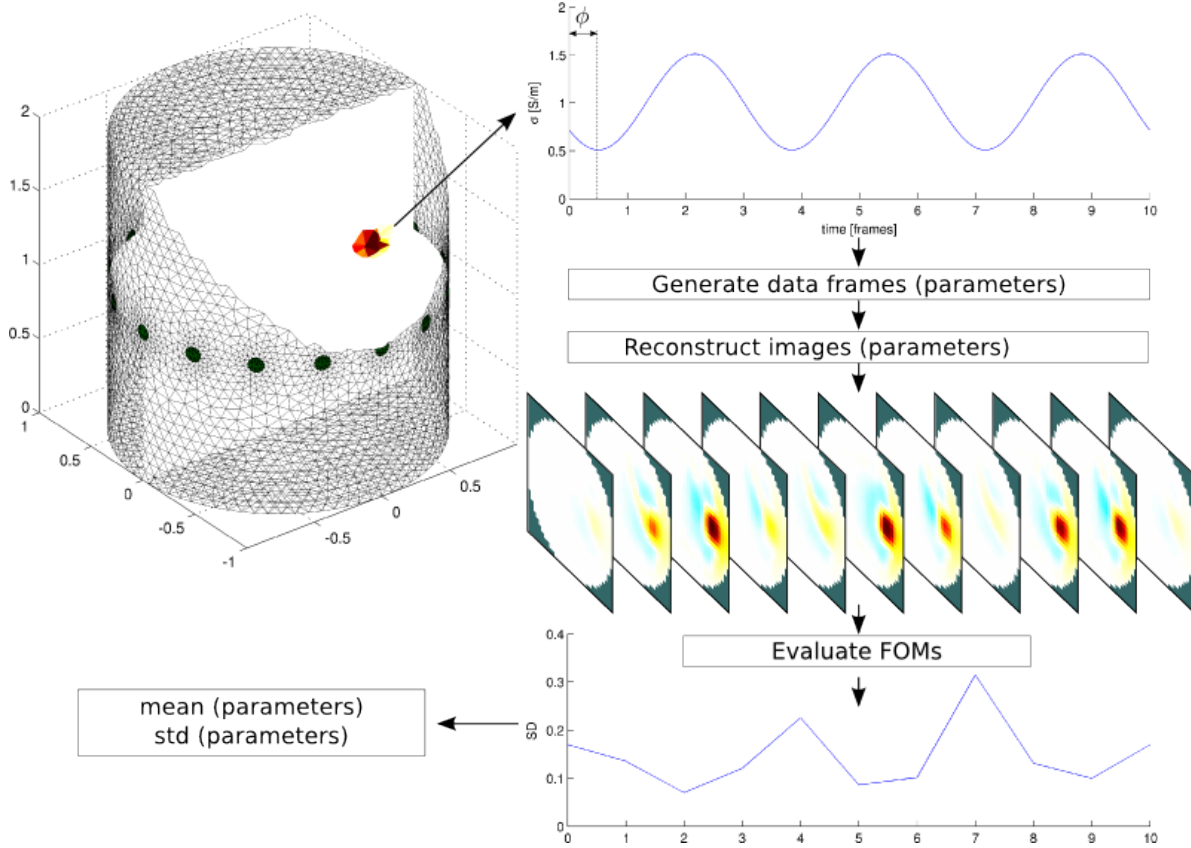


Figure 2. Overview of the proposed methodology. Data are simulated (FEM model, top left) for a contrast which varies over time (top right), and then reconstructed into an image sequence (right middle) from which temporal figures of merit (bottom right) are calculated. For each choice of data generation (e.g. frequency, phase) and image reconstruction (i.e. choice of algorithm and its parameters) parameters, the mean \pm std of each FOM are calculated.

Mean and standard-deviation for each of the FOM are then computed over the n_f FOM values obtained for the n_f frames. Figure 2 summarizes the methodology used for all simulations.

For each simulation set, a radius r , frequency f_f , phase ϕ , number of cycles n_c and SNR is set. One of the following parameter is then varied over a range of reasonable values: 1) number of cycles, 2) frequency, 3) phase, 4) radius, 5) SNR, and 6) algorithm hyperparameter. If unspecified, the algorithm hyperparameter has been set according to the noise figure method to obtain a noise figure of 0.5 (Graham and Adler 2006). Three reconstruction algorithms have been considered: 1) Gauss-Newton ($\lambda = 0.0453$ with a 0.5-exponent NOSER prior (Cheney *et al* 1990)), 2) temporal ($d = 3$, $\gamma = 0.8$, $\lambda = 0.0453$ with a 0.5-exponent NOSER prior) and 3) Kalman filter ($\lambda = 0.0453$ with a 0.5-exponent NOSER prior). For the Kalman filter, 100 dummy frames (in which the target conductivity followed (24)) were added at the beginning of the simulation in order for the Kalman filter performance to stabilize.

3. Results

Simulations of FOM for all combinations of the three reconstruction algorithms and three types of EIT data frames have been performed. Complete simulation results are available in the electronic supplement which also includes additional results for two extra reconstruction algorithms: Backprojection and GREIT. In the next sections, only significant results about the effects of the number of cycles, frequency, phase, radius, SNR, and hyperparameter are discussed and presented for selected reconstruction algorithms and types of EIT data frames.

3.1. Number of Cycles

The FOM were analysed as a function of the number of cycles. Clearly, the FOM for Gauss-Newton are not affected by the number of cycles. For the temporal reconstruction algorithm, small variations were observed for the SD mean and all standard-deviations except for TAR for less than 3 cycles. For the Kalman filter, despite the fact that 100 dummy frames were used for stabilization purposes, there is a significant dependence on the number of cycles and some parameters, such as TAR and RNG, do not seem to reach a plateau even for 32 cycles. This is mainly due to the parameter we use for the Kalman filter that provides a significant amount of temporal correlation. The behaviour of the Kalman filter is similar in this case to what happens for an infinite impulse response (IIR) filter. For the rest of the simulations, we elected to use four as the number of cycles, which seems reasonable for most reconstruction algorithms, Kalman filter being the only exception.

3.2. Frequency

Figure 3 shows FOM calculated as a function of frequency for the Gauss-Newton algorithm for three different types of EIT data frames. For perfect EIT data frames, FOM are, of course, independent of frequency. For interpolated EIT data frames, FOM are always closer to those of the perfect data frames except for TAR where the interpolation actually worsened the FOM. This peculiar behaviour can be better understood by looking at figure 1(b) where it can be seen that TAR actually improves for interpolated frames when the value of the conductivity target is large but worsened when it is small. So the accuracy of the amplitude over an entire sinusoidal cycle is worse for interpolated frames than for realistic frames. As expected, FOM worsened for realistic and interpolated frames as the frequency of the conductivity variations increases. For realistic frames, frequencies as small as 0.01 cycles/frame still produce some variations in FOM which is especially obvious while looking at the standard-deviations of FOM.

3.3. Phase

Phase (ϕ from (24)) represents the phase shift between the conductivity variation of the target and the beginning of the first EIT frame. All FOM were affected in a periodic way

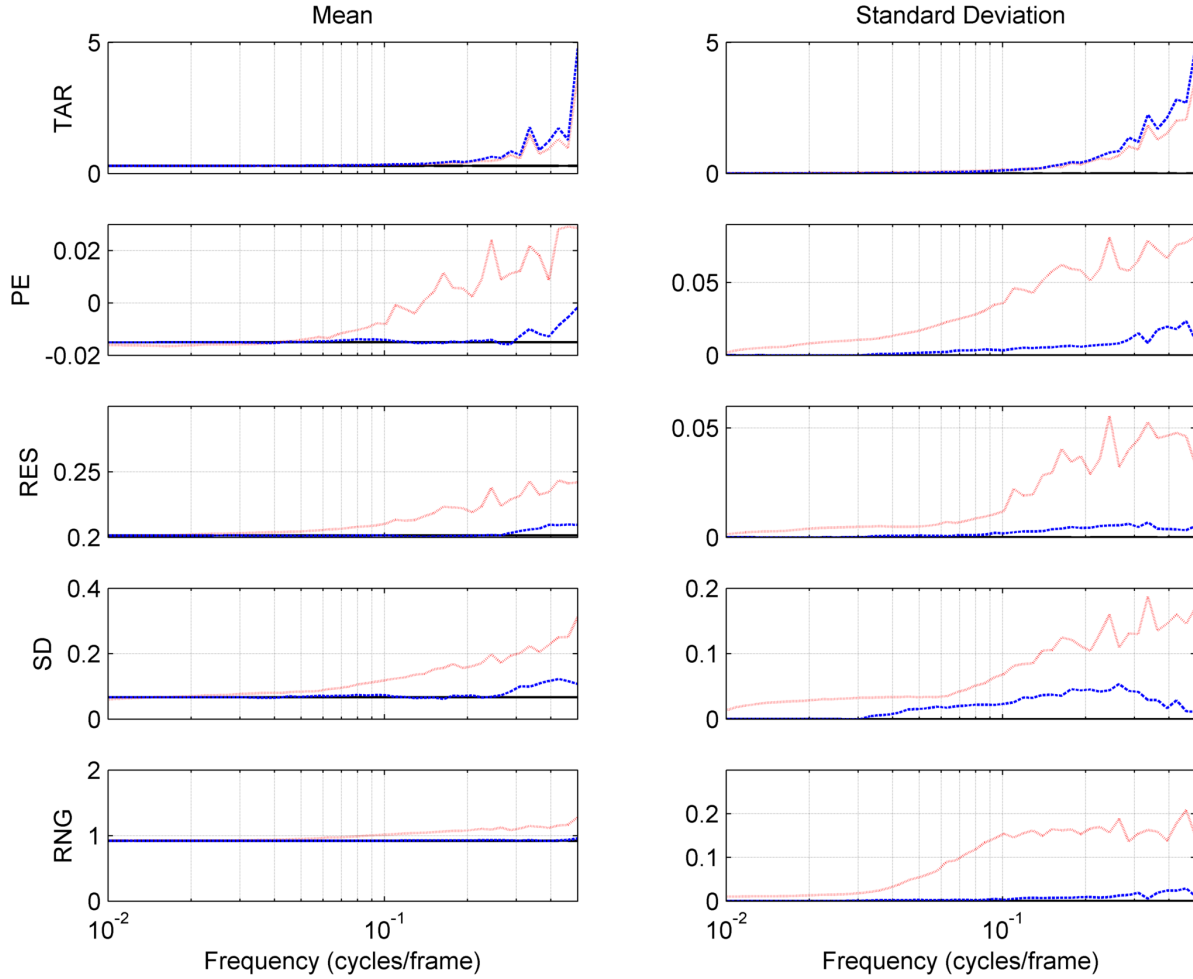


Figure 3. Temporal FOM as a function of frequency for Gauss-Newton reconstruction algorithm using perfect (—), realistic (⋯⋯⋯) and interpolated (- - -) frame types. (Phase = 0, Number of cycles = 4, radius = 2/3, SNR = ∞).

by the variation of phase. This can be explained by the fact that the 208 measurements are made in a given sequence and some measurements are more sensitive to the selected conductivity target location than others. If the target conductivity is smallest or largest due to the phase shift when the most sensitive measurements are made, this will greatly affect the FOM values. For the Kalman filter, the FOM are relatively independent of phase except for TAR. For the Gauss-Newton algorithm, most FOM exhibit a periodic behaviour except for RES. The temporal reconstruction algorithm exhibits a relatively periodic behaviour except it seems more erratic for small phase values for PE and SD.

3.4. Radius

Figure 4 shows FOM calculated as a function of radius for the Gauss-Newton algorithm for three different types of EIT data frames. In general, the FOM for perfect frames are better than those for interpolated frames which are better than those for realistic frames. The only exception is TAR when the conductivity target is located between

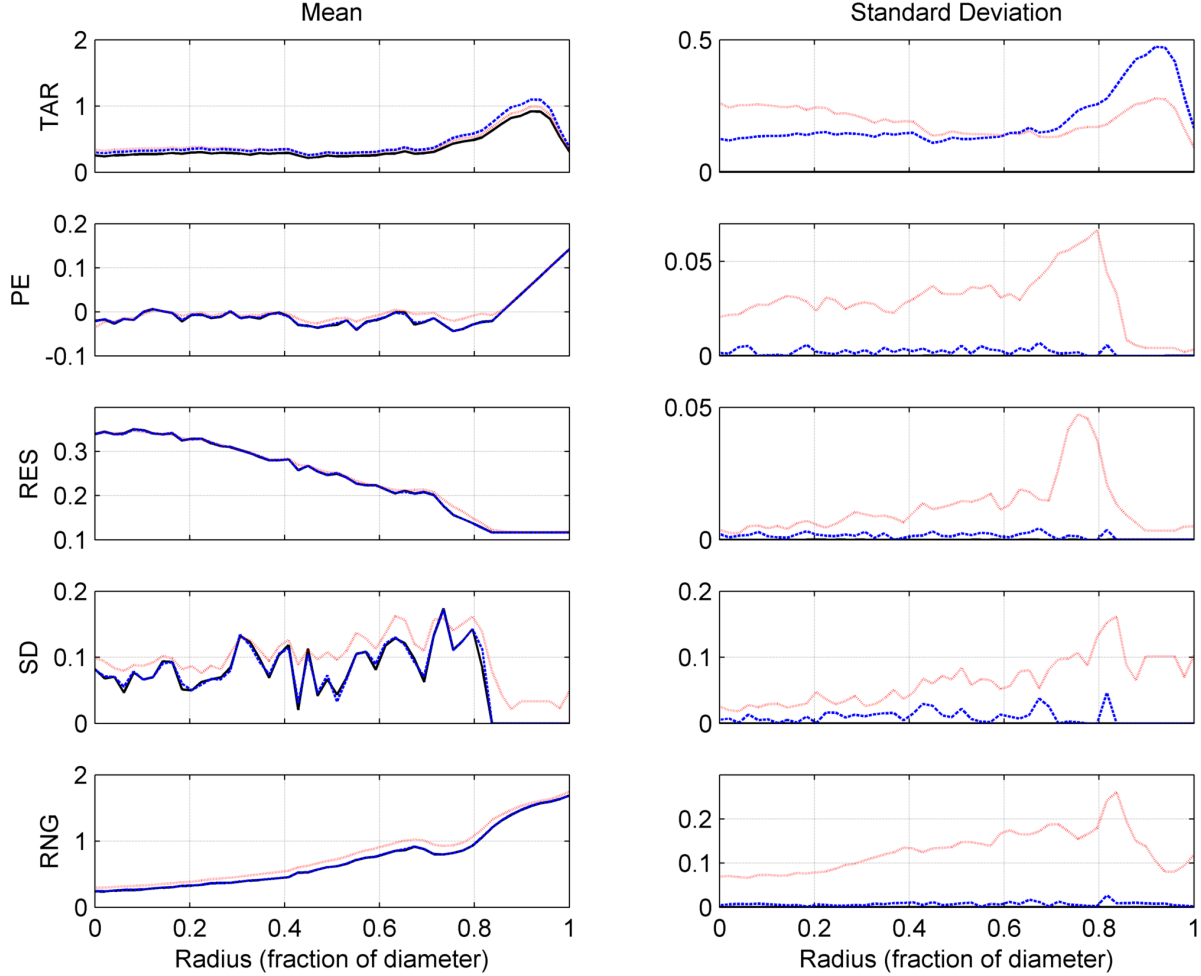


Figure 4. Temporal FOM as a function of radius for Gauss-Newton reconstruction algorithm using perfect (—), realistic (⋯⋯⋯) and interpolated (- - -) frame types. (Frequency = 0.1 cycles/frame, Phase = 0, Number of cycles = 4, SNR = ∞).

about 0.7 and 1.0, close to the medium boundary. In these locations, interpolation seems to worsen the amplitude response. There is a sharp change in FOM behaviour for the region where the radius is between 0.8 and 1.0. The RNG and PE is worst but the TAR, RES and SD is best.

3.5. SNR

SNR was calculated as a ratio of the amplitude of the difference signal $\mathbf{y} = (\mathbf{v} - \mathbf{v}_r)$, and varied from 10^{-1} to 10^4 . In this case, simulations were performed for a frequency of 0 cycles/frame which means that the conductivity target was not varying as a function of time. Only the noise was varied as a function of time and, in this case, the number of cycles (100) means the number of random noise vectors that were considered for the mean and standard-deviation calculations. Figure 5 shows FOM calculated as a function of SNR for three different reconstruction algorithms with realistic data frames. Most performance indicators behave as a sigmoid function with two plateaus and varies

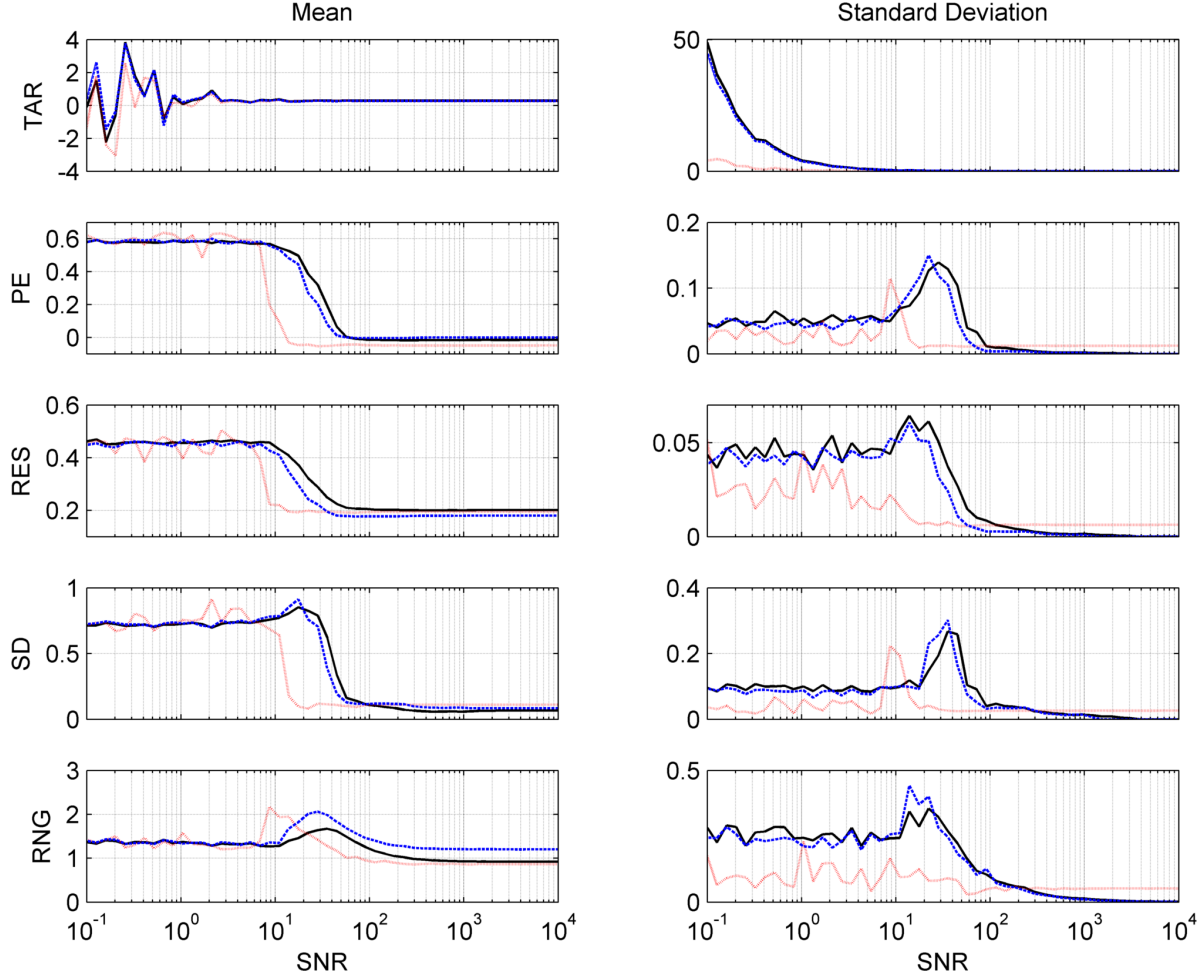


Figure 5. Temporal FOM as a function of SNR for Gauss-Newton (—), Kalman (.....) and temporal (- - -) reconstruction algorithms using realistic frame type. (Frequency = 0 cycles/frame, Phase = 0, Number of cycles = 100, radius = 2/3).

sharply in between. The Kalman filter however is able to maintain its high performance for much lower SNR than the temporal reconstruction algorithm which is itself better than Gauss-Newton. For very low SNR, the performance of the Kalman filter are however more erratic than those of the other two algorithms that are more constant in this low-SNR region.

3.6. Hyperparameter

For the Gauss-Newton and temporal algorithms, as hyperparameter value is increased, FOM reach a plateau where TAR is maximal, PE is relatively small, RES is worst, SD is worst, and RNG is best. The behaviour of both algorithms is about the same except in the case of the temporal algorithm where TAR mean and standard-deviation values are higher for higher values of the hyperparameter. The behaviour for Kalman is very different than the other two algorithms. For instance, FOM reach no plateaus as hyperparameter increases. This peculiar behaviour for Kalman is probably explainable

by the fact that only one hyperparameter controls both spatial and time correlations which both affects FOM but in a different way.

4. Discussion and Conclusion

This paper considers the problems caused by the assumption that EIT data in each frame are recorded at the same instant. We have developed a framework to evaluate reconstruction algorithms as a function of various temporal characteristics of the EIT data. Simulations have been performed to apply those FOM on a combination of three reconstruction algorithms and three EIT data types. Extensive comparisons are provided and made available in the electronic supplement. Results show that the FOM are mainly sensitive to the reconstruction algorithm, the parameters of the reconstruction algorithm, the position of the small conductive target as well as the frequency and phase of the change of the conductivity of the target. The same FOM can be used to assess pure SNR performance when the frequency is set to zero.

Our results show that artefacts due to the temporal nature of EIT data occur much earlier than previously thought. Frequency-related artefacts have been observed at frequencies lower than one tenth of the frame rate. These results support the recommendation of Yerworth and Bayford (2013) that a frame rate of at least 50 times higher than the highest frequency component should be used if no temporal reconstruction or interpolation techniques are used. Imaging results also show that previously observed artefacts in images with different reconstruction algorithms might be due to the fact that we are trying to image changes of conductivity that are at the limit of being too fast to be observed. This phenomenon could be better understood as an imaging equivalent to the aliasing that occurs during signal processing with insufficient sample rate.

With this comparison framework, we simulate a sinusoidally varying conductivity target at different locations and frequencies. In practice, however, breathing and cardiac activities produce much more complex conductivity variations. The lungs and heart external surfaces are expanding and contracting during breathing and cardiac activities. The change in conductivity is also not purely sinusoidal as several harmonics would have to be considered to simulate the cardiac and lung related conductivity variations. The comparison framework however presents a simple yet useful scenario to quantitatively assess reconstruction techniques.

So far, it is impossible to declare a clear winner between the interpolation technique, the Kalman filter and the temporal filter as they all have exhibited strengths and weaknesses in different areas as shown in the FOM results. Furthermore, the parameters of each algorithm could have been optimized to improve performance of any particular FOM. The main point of this paper was rather to provide a platform for comparing temporal reconstruction algorithms including 1) a target with sinusoidally varying conductivity variation, 2) five FOM whose mean and standard-deviation have to be calculated and 3) three types of EIT data frames. We showed that it can be

applied with different temporal reconstruction algorithms. We thus recommend this comparison framework as a tool for developing future generations of optimized temporal reconstruction algorithms and will make it publicly available through EIDORS.

Acknowledgments

This work is supported in part by the Natural Sciences and Engineering Research Council of Canada (NSERC).

References

- Adler A, Amato M B, Arnold J H, Bayford R, Bodenstern M, Böhm S H, Brown B H, Frerichs I, Stenqvist O, Weiler N and Wolf G K 2012 Whither lung EIT: where are we, where do we want to go and what do we need to get there? *Physiol. Meas.* **33** 679-94
- Adler A, Arnold J H, Bayford R, Borsic A, Brown B, Dixon P, Faes T J, Frerichs I, Gagnon H, Gärber Y, Grychtol B, Hahn G, Lionheart W R, Malik A, Patterson R P, Stocks J, Tizzard A, Weiler N and Wolf G K 2009 GREIT: a unified approach to 2D linear EIT reconstruction of lung images *Physiol. Meas.* **30** S35-55
- Adler A, Dai T and Lionheart W R B 2007 Temporal image reconstruction in electrical impedance tomography *Physiol. Meas.* **28** S1-11
- Adler A and Guardo R 1996 Electrical impedance tomography: regularized imaging and contrast detection *IEEE Trans. Med. Imaging* **15** 170-9
- Cheney M, Isaacson D, Newell J C, Simske S and Goble J C 1990 NOSER: an algorithm for solving the inverse conductivity problem *Int. J. Imaging Syst. Technol.* **2** 66-75
- Dräger AG 2010 Technical data sheet: PulmoVista 500, Lübeck, Germany
- Graham B M and Adler A 2006 Objective selection of hyperparameter for EIT *Physiol. Meas.* **27** S65-79
- Kim B S, Kim K Y, Kao T-J, Newell J C, Isaacson D and Saulnier G J 2006 Dynamic electrical impedance imaging of a chest phantom using the Kalman filter *Physiol. Meas.* **27** S81-91
- McCann H, Ahsan, S T, Davidson J L, Robinson R L, Wright P and Pomfrett C J D 2011 A portable instrument for high-speed brain function imaging: FEITER *Conf Proc IEEE Eng Med Biol Soc.* 2011:7029-32.
- Swisstom AG 2014 Swisstom BB² Product Information 2ST100-112, Rev. 000, Landquart, Switzerland
- Trigo F C, Gonzalez-Lima R and Amato M B P A 2004 Electrical impedance tomography using the extended Kalman filter *IEEE Trans. Biomed. Eng.* **51** 72-81
- Vauhkonen M, Karjalainen P A and Kaipio J P 1998 A Kalman Filter Approach to Track Fast Impedance Changes in Electrical Impedance Tomography *IEEE Trans. Biomed. Eng.* **45** 486-93
- Voutilainen A, Lipponen A, Savolainen T, Lehtikainen A, Vauhkonen M and Kaipio J P 2012 Fast Adaptive 3-D Nonstationary Electrical Impedance Tomography Based on Reduced-Order Modeling *IEEE Trans. Instrum. Meas.* **61** 2665-81
- Yerworth R and Bayford R 2013 The effect of serial data collection on the accuracy of electrical impedance tomography images *Physiol. Meas.* **34** 659-69